Co-Optimizing Synthetic and Synchronous Inertia in Frequency-Constrained Unit Commitment: A Case Study on La Palma

Azeez O. Olasoji
Department of Electrical Engineering
University of Cape Town
Cape Town, South Africa
olsaze001@myuct.ac.za

David T.O. Oyedokun
Department of Electrical Engineering
University of Cape Town
Cape Town, South Africa
david.oyedokun@uct.ac.za

Adebayo Adeyinka V
Department of Electrical Engineering
University of Johannesburg
Johannesburg, South Africa
avadebayo@uj.ac.za

Mohammad Rajabdorri
IIT, ETSI-ICAI
Universidad Pontificia Comillas
Madrid, Spain
mrajabdorri@comillas.edu

Juan Esteban Sierra-Aguillar
Department of Electrical Engineering
Universidad de Antioquia
Medellin, Colombia
juane.sierra@udea.edu.co

Akinola Ajayi-Obey
School of Engineering
University of Warwick, Coventry
Coventry, United Kingdom
akinola.ajayi-obe@warwick.ac.uk

Pelumi Peter Aluko-Olokun
Department of Electrical Engineering
Sheffield Hallam University
Sheffield, United Kingdom
Pelumialukoolokun@ieee.org

2026 IEEE Texas Power and Energy Conference (TPEC) | 979-8-3315-5720-1/26/$31.00 ©2026 IEEE | DOI: 10.1109/TPEC67884.2026.11513199

***Abstract*—High penetrations of converter-interfaced renewable energy sources (RES) are eroding synchronous inertia in many power systems, making frequency security a binding constraint in unit commitment (UC), especially for weak island grids. This paper develops an analytical frequency-constrained unit commitment (FCUC) formulation that (i) co-optimises synchronous inertia and synthetic inertia (SI) from wind power plants and (ii) supports both classical DC power-flow and PTDF-based linear sensitivity factor (LSF) network representations within a unified mixed-integer linear programming (MILP) framework. The frequency nadir constraints is enforced via a separable-programming approximation that remains fully MILP-compatible. The model is validated on the real La Palma island system. Results show that, under an unconstrained network (transmission-capacity factor $\mathrm{TCF} = 1.0$), varying the emulated inertia constant k^{em} between 0 s and 6 s has negligible impact on total cost, renewable spillage, and frequency-security indicators: RoCoF remains orders of magnitude below its limit and the nadir constraint is numerically binding in all cases. A comparison between DC and LSF formulations confirms that the LSF model closely reproduces the DC dispatch and frequency metrics while achieving smaller optimality gaps. A subsequent TCF evaluation shows that tightening transmission limits only becomes economically material at $\mathrm{TCF} = 0.6$, where costs rise and a small amount of RES curtailment appears, without compromising RoCoF or nadir security. Overall, the results demonstrate that SI from wind can be co-optimised with synchronous inertia and LSF-based transmission constraints in a single tractable FCUC model, providing a structured way to assess inertia provision, wind utilisation, and congestion management in low-inertia island grids.**

***Index Terms*—Frequency-constrained unit commitment (FCUC), synthetic inertia (SI), wind power, renewable energy integration, mixed-integer linear programming (MILP), low-inertia systems, and power system optimisation.**

NOMENCLATURE

Sets and indices

- i Index of generating units, $i = 1, \ldots, I$.
- t Index of time periods (hours), $t = 1, \ldots, T$.
- s Index of buses, $s = 1, \ldots, S$.
- ℓ Index of transmission lines, $\ell = 1, \ldots, L$.
- r Index of inertia grid points in the SP nadir approximation.
- q Index of reserve grid points in the SP nadir approximation.
- k Index of outage (contingency) grid points in the SP nadir approximation.

Decision variables

- $x_{t,i}$ Commitment of unit i at time t (1 if online, 0 otherwise).
- $y_{t,i}, z_{t,i}$ Start-up and shut-down indicators of unit i at time t.
- $g_{t,i}$ Power output of generator i at time t [MW].
- $r_{t,i}$ Primary reserve provided by generator i at time t [MW].
- $\theta_s(t)$ Voltage angle at bus s at time t [rad].
- $f_\ell(t)$ Active power flow on line ℓ at time t [MW].
- $P_s^{\mathrm{net}}(t)$ Net injection at bus s at time t (generation + wind − demand) [MW].

979-8-3315-5720-1/26/$31.00 © 2026 IEEE

Authorized licensed use limited to: UNIVERSIDAD PONTIFICIA DE COMILLAS. Downloaded on June 29,2026 at 06:40:54 UTC from IEEE Xplore. Restrictions apply.

- $\text{curt}(t)$ Curtailed wind power at time t [MW].
- $p_{\text{SI}}(t)$ Synthetic-inertia headroom scheduled from wind at time t [MW].
- $H_{\text{SI}}(t)$ Synthetic inertia contribution from wind at time t [s].
- $H_{\text{tot}}(t)$ Total system inertia (synchronous + synthetic) at time t [s].
- $\lambda^{H}_{t,r}$ Convex-combination weight for inertia grid point r at time t.
- $\lambda^{R}_{t,q}$ Convex-combination weight for reserve grid point q at time t.
- $\lambda^{P}_{t,k}$ Convex-combination weight for outage grid point k at time t.

Parameters and constants

- $\text{suc}_{t,i}$ Start-up cost of unit i at time t [€].
- $\text{gc}_{t,i}$ Generation cost of unit i at time t [€].
- $D_s(t)$ Demand at bus s at time t [MW].
- $P_{\text{wind}}(t)$ Available wind power at time t [MW].
- $A^{g}_{s,i}$ Incidence (connection) of generator i at bus s (1 if connected, 0 otherwise).
- $\text{PTDF}_{\ell,s}$ Power transfer distribution factor from bus s on line ℓ [–].
- $\underline{G}_i, \overline{G}_i$ Minimum and maximum power output of generator i [MW].
- $\underline{R}_i, \overline{R}_i$ Ramp-down and ramp-up limits of generator i [MW/h].
- $g_i^{\text{on-off}}$ Initial on/off status of generator i.
- $L_i^{\text{up,min}}, L_i^{\text{down,min}}$ Minimum up/down times of generator i [h].
- $F_\ell^{\max}$ Thermal capacity of line ℓ [MW].
- TCF Transmission-capacity factor applied to $F_\ell^{\max}$ [–].
- B_ℓ Series susceptance of line ℓ [p.u.].
- H_i Inertia constant of generator i [s].
- M_i MVA base (rating) of generator i [MVA].
- f_0 Nominal system frequency [Hz].
- D_{load} Load-damping coefficient used in the nadir and QSS constraints [p.u./Hz].
- P_D Total system demand used in the swing-equation approximation [MW].
- T_g Effective governor (reserve deployment) time constant [s].
- k^{em} Emulated inertia constant mapping $p_{\text{SI}}(t)$ to $H_{\text{SI}}(t)$ [s].
- η_{SI} Maximum fraction of non-curtailed wind power available for SI headroom [–].
- $P_L(t)$ Largest credible generation loss (contingency size) at time t [MW].
- $\Delta f^{\max}_{\text{RoCoF}}$ Maximum admissible RoCoF [Hz/s].
- $\Delta f^{\max}_{\text{QSS}}$ Maximum admissible QSS frequency deviation [Hz].
- $\Delta f_{\max}$ Maximum admissible frequency-nadir deviation [Hz].
- H_r^{grid} Inertia grid point r used in the SP nadir approximation [s].
- R_q^{grid} Reserve grid point q used in the SP nadir approximation [MW].
- P_k^{grid} Outage grid point k used in the SP nadir approximation [MW].
- α, β Scaling constants used in the SP mapping between $(H_{\text{tot}}, \sum_i r_{t,i})$ and the grid variables.

I. Introduction

High penetrations of converter-interfaced renewable energy sources (RES) have accelerated the erosion of synchronous inertia in modern power systems. This trend is especially critical in isolated grids such as La Palma, where the loss of a single synchronous unit can produce large frequency excursions due to limited inertia and restricted interconnection support [1]. Ensuring frequency security under these conditions requires commitment and dispatch decisions that explicitly account for inertia availability and primary frequency-response capabilities.

Analytical frequency-constrained unit commitment (FCUC) formulations have recently emerged as a tractable means of embedding frequency-security considerations directly into the UC problem. These formulations capture key metrics such as Rate of Change of Frequency (RoCoF), frequency nadir, and quasi-steady-state (QSS) deviation without resorting to full dynamic simulations. A notable example is the PTDF-based FCUC framework in [2], which incorporates linear sensitivity factors (LSFs) to enforce transmission constraints while maintaining computational efficiency. However, that formulation assumes that all inertia is supplied by synchronous generators, thereby excluding the fast active-power injection capabilities of modern wind power plants (WPPs).

This assumption is increasingly limiting. Contemporary Type-3/Type-4 WPPs can provide synthetic inertia (SI) through fast frequency-response controllers, emulating the inertial power surge characteristic of synchronous machines. Evidence from islanded systems such as La Palma and Tenerife shows that WPPs can contribute meaningfully to both reserve provision and early frequency support when appropriately deloaded and controlled [3]. Yet, despite this operational relevance, the joint optimisation of synchronous inertia, synthetic inertia, and transmission constraints has not been integrated into analytical FCUC models.

This study addresses this gap by developing an enhanced FCUC formulation that co-optimises synchronous and synthetic inertia within the FCUC framework. The model employs a separable-programming (SP) linearisation of the frequency-nadir constraint that remains fully MILP-compatible as seen in [4], [5], enabling scalable solution under practical time limits. Two alternative network representations are supported: a classical DC power-flow (DCPF) model and a PTDF-based LSF model that facilitates congestion analysis under transmission-capacity de-rating.

The contributions of this work are threefold:

1) An MILP-compatible analytical FCUC formulation that co-optimises synchronous inertia and synthetic inertia

Authorized licensed use limited to: UNIVERSIDAD PONTIFICIA DE COMILLAS. Downloaded on June 29,2026 at 06:40:54 UTC from IEEE Xplore. Restrictions apply.

from WPPs using a separable-programming approximation of the frequency-nadir constraint.
2) A unified framework that supports both DC and PTDF-based LSF transmission models, and a demonstration that both produce near-identical frequency-security behaviour (RoCoF, nadir, QSS) when the network is unconstrained.
3) A quantitative analysis on the La Palma system showing how synthetic inertia provision and transmission-capacity de-rating jointly influence operating cost, renewable spillage, frequency-security margins, and congestion.

The remainder of this paper is organised as follows. Section II reviews FCUC methods, synthetic inertia modelling, and LSF-based transmission representations. Section III presents the proposed formulation, including the classical UC model, the DC and LSF network representations, and the analytical frequency constraints. Section IV reports case-study results for La Palma under varying synthetic inertia constants and transmission-capacity factors. Section V summarises key findings and outlines future research directions .

II. Background and Related Work

Low-inertia grids with high penetrations of inverter-based RES face increased risk of large RoCoF, deep frequency nadirs, and quasi-steady-state (QSS) deviations following contingencies [1], [5]. Frequency-constrained unit commitment (FCUC) models address this by embedding frequency-security criteria directly into the UC problem. Existing FCUC formulations broadly fall into two groups: *analytical* approaches, which derive RoCoF, nadir, and QSS constraints from the swing equation and linearise them using techniques such as separable programming, piecewise linearisation, or bounding [4], [6], [7]; and *data-driven* approaches, which use machine-learning surrogates (e.g., logistic regression, SVMs, or GNNs) to preserve MILP tractability while reducing modelling effort [5], [8].

In parallel, network-constrained UC and SCUC models typically represent transmission either via DC power flow (DCPF) with bus angles or via power transfer distribution factors (PTDFs) or linear sensitivity factors (LSFs) that map nodal injections to line flows in a scalable way [2], [9], [10]. Most analytical FCUC studies either neglect transmission limits or use simplified DCPF constraints, treating frequency security and congestion management separately. The PTDF-based FCUC formulation in [2] is a recent step towards unifying analytical frequency constraints and LSF-based transmission modelling, but it assumes purely synchronous inertia and does not account for synthetic inertia from RES.

Synthetic inertia (SI) from Type-3/Type-4 wind turbines has been extensively studied at the controller and dynamic-simulation level [3], [11]. To the best of the authors' knowledge, [4] is one of the few analytical FCUC formulations that embeds SI via a separable-programming nadir approximation in a MILP-compatible framework, but it is limited to a single DCPF representation on a large meshed system. This paper builds on [2], [4] by co-optimising synchronous and synthetic inertia within a unified FCUC model that supports both DCPF and PTDF-based LSF transmission representations and is validated on a low-inertia island system.

III. Methodology

This section presents the proposed frequency-constrained unit commitment (FCUC) formulation. The model retains a classical MILP-based UC core and augments it with (i) two alternative transmission representations—DC power flow and PTDF-based linear sensitivity factors (LSFs)—and (ii) analytical frequency-security constraints incorporating synchronous and synthetic inertia. All constraints are MILP-compatible and identical across the DC and LSF variants, except for the transmission block.

A. Classical Unit Commitment Formulation

The FCUC model retains a standard MILP-based UC core. The objective minimises start-up and generation costs:

$$\min_{x,y,z,g,r} \sum_{t\in T}\sum_{i\in I} \left(\mathrm{suc}_{t,i} + \mathrm{gc}_{t,i}\right). \tag{1}$$

This objective is subject to textbook UC constraints on commitment logic, minimum up/down times, capacity limits, and ramping, e.g.,

$$x_{t,i} - x_{t-1,i} = y_{t,i} - z_{t,i}, \quad \forall t, i, \tag{2}$$

$$\underline{G}_i x_{t,i} \le g_{t,i} \le \overline{G}_i x_{t,i}, \quad \forall t, i, \tag{3}$$

$$g_{t,i} - g_{t-1,i} \le \overline{R}_i, \quad g_{t-1,i} - g_{t,i} \le \underline{R}_i, \quad \forall t, i, \tag{4}$$

together with minimum up/down time constraints as in conventional UC formulations (see, [1], [2] for more details). Reserve variables $r_{t,i}$ are defined in the usual way and are linked to the frequency-security constraints described below. Also, Wind power is treated as a non-dispatchable resource subject to curtailment $\mathrm{curt}(t)$, and total demand at each time period is enforced through the transmission block described next.

B. Transmission Modelling

As stated prior, two network formulations are supported.

1) DC Power-Flow Formulation: Bus voltage angles $\theta_s(t)$ determine line flows:

$$f_\ell(t) = B_\ell \left(\theta_{m(\ell)}(t) - \theta_{n(\ell)}(t)\right), \tag{5}$$

with thermal limits $|f_\ell(t)| \le F_\ell^{\max}$. A slack bus is fixed to ensure angle reference. Power balance at each bus is:

$$\sum_i A^g_{s,i} g_{t,i} + P_s^{\mathrm{wind}}(t) - D_s(t) = \sum_{\ell\in L_s} f_\ell(t). \tag{6}$$

Authorized licensed use limited to: UNIVERSIDAD PONTIFICIA DE COMILLAS. Downloaded on June 29,2026 at 06:40:54 UTC from IEEE Xplore. Restrictions apply.

2) PTDF-Based LSF Formulation: Net injections are:

$$P_s^{\text{net}}(t) = \sum_i A_{s,i}^g g_{t,i} + P_s^{\text{wind}}(t) - D_s(t). \tag{7}$$

Power balance imposes:

$$\sum_s P_s^{\text{net}}(t) = 0. \tag{8}$$

Line flows are computed via PTDF factors:

$$-F_\ell^{\max} \cdot \text{TCF} \le \sum_s \text{PTDF}_{\ell,s}\, P_s^{\text{net}}(t) \le F_\ell^{\max} \cdot \text{TCF}, \tag{9}$$

where the transmission-capacity factor TCF $\in \{1.0, 0.9, 0.8\}$ enables controlled de-rating. This formulation eliminates voltage-angle variables and mirrors the structure of Code B.

C. Frequency-Security Constraints with Synthetic Inertia

Frequency response is modelled using standard swing-equation-based criteria on RoCoF, nadir, and quasi-steady-state (QSS) deviation [1], [4]. The total inertia at time t combines synchronous and synthetic contributions:

$$H_{\text{tot}}(t) = \sum_{i \in I} H_i M_i x_{t,i} + H_{\text{SI}}(t), \tag{10}$$

where synthetic inertia is provided by deloaded wind power as

$$0 \le p_{\text{SI}}(t) \le \eta_{\text{SI}} \big(P_{\text{wind}}(t) - \text{curt}(t)\big), \tag{11}$$

$$H_{\text{SI}}(t) = k^{\text{em}}\, p_{\text{SI}}(t), \tag{12}$$

with η_{SI} the SI headroom factor and k^{em} the emulated inertia constant.

The RoCoF constraint enforces a minimum inertia level for a given largest credible loss $P_L(t)$:

$$H_{\text{tot}}(t) \;\ge\; \frac{P_L(t) f_0}{2\,\Delta f_{\text{RoCoF}}^{\max}}, \quad \forall t. \tag{13}$$

Steady-state (QSS) frequency security is imposed via a minimum reserve requirement:

$$\sum_{i \in I} r_{t,i} \;\ge\; P_L(t) - D_{\text{load}}\, \Delta f_{\text{QSS}}^{\max}, \quad \forall t, \tag{14}$$

where D_{load} denotes the load-damping factor.

The nadir constraint couples inertia, primary reserve, and outage size. Following [4], we approximate the nadir condition using a separable-programming (SP) scheme. The post-contingency inertia and reserve are projected onto fixed grids $\{H_r^{\text{grid}}\}$ and $\{R_q^{\text{grid}}\}$, and the outage size onto $\{P_k^{\text{grid}}\}$, with associated convex-combination weights $\lambda_{t,r}^H$, $\lambda_{t,q}^R$, and $\lambda_{t,k}^P$. Substituting these into the analytical nadir expression yields the linear inequality

$$\frac{\sum_r \big(H_r^{\text{grid}}\big)^2 \lambda_{t,r}^H - \sum_q \big(R_q^{\text{grid}}\big)^2 \lambda_{t,q}^R}{\alpha\beta} - \frac{f_0 T_g}{4\,\Delta f_{\max}} \sum_k \big(P_k^{\text{grid}}\big)^2 \lambda_{t,k}^P + \frac{D_{\text{load}}\, d(t)\, f_0 T_g}{4}\, P_L(t) \;\ge\; 0, \tag{15}$$

where α and β are scaling constants. Hence, the FCUC model remains fully MILP-compatible. The same frequency-security block is used in both the DC and PTDF-based LSF variants.

TABLE I
DC ANALYTICAL FCUC RESULTS VS. k^{EM} (TCF = 1.0)

k^{em} [s]	Cost [k€]	Spill. [MWh]	Run-time [s]	Opt. gap [%]	Min nadir margin [Hz]	Max RoCoF [Hz/s]
0	122.4	0	11,012	0.76	-1.6×10^{-12}	9.3×10^{-4}
2	122.7	0	11,347	0.98	-1.6×10^{-12}	9.3×10^{-4}
4	131.5	0	11,202	7.9	-1.56×10^{-12}	9.3×10^{-4}
5	122.3	0	12,010	0.62	-3.36×10^{-12}	9.2×10^{-4}
6	123.0	0	12,010	1.00	-4.12×10^{-12}	9.2×10^{-4}

IV. CASE STUDY AND RESULTS

A. La Palma System and Simulation Setup

This study uses the real-world configuration of the La Palma island grid—part of Spain's Canary Islands—to evaluate frequency-constrained unit commitment under low-inertia conditions. The system is weakly interconnected, making it particularly vulnerable to frequency instability during contingencies. In 2018, La Palma's energy needs were met primarily by eleven conventional generators, supplying an average hourly demand of 31.7 MWh and a total annual consumption of approximately 277.8 GWh. While the island has 117.7 MW of installed capacity, only about 6% is from wind power, and roughly 10% of yearly demand is met by renewable sources [5].

All scenarios are solved with the same UC and frequency-constraint parameters; only the network representation (DC versus PTDF-based LSF), the emulated inertia constant k^{em}, and the transmission-capacity factor TCF are varied. Synthetic inertia from wind is enabled in all runs, with the SI headroom limited to a fraction η_{SI} of available (non-curtailed) wind power as described in Section III. The following scenario sets are considered:

- **DC analytical FCUC**: $k^{\text{em}} \in \{0, 2, 4, 5, 6\}$ with TCF $= 1.0$;
- **LSF FCUC, equivalence check**: DC versus LSF comparison at $k^{\text{em}} = 4$ s and TCF $= 1.0$;
- **LSF FCUC, TCF sweep**: $k^{\text{em}} = 4$ s with TCF $\in \{1.0, 0.9, 0.8, 0.6\}$.

For each case, we extract total cost, RES spillage, optimality gap, runtime, frequency-security indicators (minimum nadir margin and maximum RoCoF), and simple congestion metrics (number of congested lines and congested line-hours) for the LSF runs. For each scenario, we report: (i) minimum nadir margin, (ii) maximum RoCoF, (iii) minimum QSS margin, (iv) total cost, RES spillage, runtime, and MILP optimality gap, and (v) simple congestion metrics (number of congested lines and congested line-hours for the LSF runs).

B. Impact of Synthetic Inertia in the DC Analytical FCUC

We first analyse the impact of varying the synthetic inertia constant k^{em} in the DC analytical FCUC formulation with TCF $= 1.0$. Table I reports total cost, RES spillage, runtime, optimality gap, and frequency-security indicators for $k^{\text{em}} \in \{0, 2, 4, 5, 6\}$, while Fig. 1 visualises the cost, optimality gap (annotated on the bars), and runtime (right axis).

Authorized licensed use limited to: UNIVERSIDAD PONTIFICIA DE COMILLAS. Downloaded on June 29,2026 at 06:40:54 UTC from IEEE Xplore. Restrictions apply.

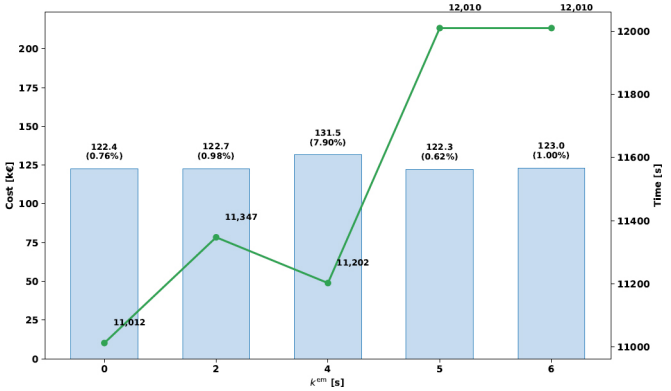


Fig. 1. DC analytical FCUC: cost (bars, with optimality gap in parentheses) and runtime (line, right axis) vs. k^{em} for $\mathrm{TCF} = 1.0$.

TABLE II
DC VS LSF FCUC AT TCF = 1.0, $k^{\mathrm{EM}} = 4$ S

Model	Cost [k€]	Spill. [MWh]	Opt. gap [%]	Min nadir margin [Hz]	Max RoCoF [Hz/s]
DC analytical	131.5	0	7.9	-1.56×10^{-12}	9.3×10^{-4}
LSF PTDF	122.3	0	1	-2.33×10^{-12}	9.2×10^{-4}

Across k^{em}, the total operating cost remains broadly stable, with values clustered around 122–123 k€ (Table I, Fig. 1). The only notable deviation occurs at $k^{\mathrm{em}} = 4$ s, where the higher reported cost coincides with a substantially larger MILP optimality gap (7.9%). This indicates that the apparent cost increase in this case is dominated by incomplete convergence, rather than a structural sensitivity to the synthetic inertia parameter.

In all cases, RES spillage is identically zero, and the maximum RoCoF is practically invariant at $\dot{f}_{\max} \approx 9.3 \times 10^{-4}$ Hz/s, i.e., far below the imposed limit. The reported nadir margins are very small negative values of order 10^{-12} Hz; these reflect numerical tolerances in the equality-form separable nadir constraint and are treated as binding rather than physical violations.

Overall, under $\mathrm{TCF} = 1.0$, varying k^{em} does not induce an observable trade-off between cost, RES utilisation, and frequency security for the La Palma operating conditions considered here.

C. DC vs LSF FCUC at TCF = 1.0

We next compare the DC analytical FCUC model with the PTDF-based LSF formulation for a representative case with $k^{\mathrm{em}} = 4$ s and $\mathrm{TCF} = 1.0$. Since transmission capacity is not de-rated, the comparison primarily tests whether the LSF representation preserves the frequency-security behaviour of the DC formulation.

Table II shows that both formulations yield zero RES spillage and nearly identical frequency-security indicators. In particular, the maximum RoCoF differs only marginally (9.3×10^{-4} vs. 9.2×10^{-4} Hz/s), and the nadir margins remain numerically close to zero.

TABLE III
IMPACT OF TCF IN LSF FCUC (LA PALMA, $k^{\mathrm{EM}} = 4$ S)

TCF [–]	Cost [k€]	Spill. [MWh]	Run-time [s]	Opt. gap [%]	Min nadir margin [Hz]	Max RoCoF [Hz/s]	# cong. lines
1.0	122.3	0	12,007	1	-2.33×10^{-12}	9.2×10^{-4}	0
0.9	122.3	0	11,615	0.6	-2.33×10^{-12}	9.2×10^{-4}	0
0.8	122.4	0	11,304	0.79	-3.12×10^{-12}	9.2×10^{-4}	0
0.6	145.4	0.89	11,479	0.95	-3.33×10^{-12}	9.2×10^{-4}	0

The DC formulation reports a higher cost than the LSF case; however, this difference aligns with the substantially larger DC optimality gap (7.9% versus 1%). The DC cost should therefore be interpreted as a loose upper bound rather than a converged optimum, whereas the LSF solution is closer to optimal. Consequently, under $\mathrm{TCF} = 1.0$, the PTDF-based LSF network model preserves the FCUC frequency behaviour observed under the DC formulation.

D. Impact of TCF in the LSF FCUC

Finally, we assess the interaction between synthetic inertia and transmission limits by varying the transmission-capacity factor in the LSF FCUC model. For $k^{\mathrm{em}} = 4$ s, the LSF formulation is solved for $\mathrm{TCF} \in \{1.0, 0.9, 0.8, 0.6\}$. Table III summarises the resulting cost, RES spillage, runtime, optimality gap, frequency-security indicators, and congestion metrics.

For $\mathrm{TCF} = 1.0$ down to 0.8, the LSF FCUC solution remains essentially unchanged: total cost stays at approximately 122.3–122.4 k€, RES spillage is zero, and the optimality gaps remain below 1%. Frequency-security indicators are also invariant across these cases, with $\dot{f}_{\max} = 9.2 \times 10^{-4}$ Hz/s and nadir margins numerically close to zero.

A clear shift occurs at $\mathrm{TCF} = 0.6$, where total cost increases to 145.4 k€ and a small amount of RES spillage (0.89 MWh) is induced. Since the MILP gap remains below 1%, this increase reflects a genuine effect of the tighter transmission limits rather than a convergence artefact. Despite this redispatch, the RoCoF and nadir indicators remain well within security limits. The congestion counter remains zero across all cases, indicating that the changes are driven by preventive operation under tighter flow limits.

V. CONCLUSION

This paper developed an analytical frequency-constrained unit commitment (FCUC) formulation for low-inertia island systems that (i) co-optimises synchronous inertia and synthetic inertia from wind power plants (WPPs) and (ii) supports both classical DC power-flow and PTDF-based linear sensitivity factor (LSF) network representations within a unified MILP framework. Frequency-security constraints on RoCoF, quasi-steady-state (QSS) deviation, and frequency nadir were enforced using a separable-programming approximation that remains fully compatible with commercial MILP solvers. The methodology was validated on the real La Palma island system.

Numerical results show that, under an unconstrained network (TCF = 1.0), varying the emulated inertia constant k^{em} between 0 s and 6 s in the DC analytical FCUC leads to almost

Authorized licensed use limited to: UNIVERSIDAD PONTIFICIA DE COMILLAS. Downloaded on June 29,2026 at 06:40:54 UTC from IEEE Xplore. Restrictions apply.

identical economic and frequency-security outcomes: total cost and RES spillage remain effectively unchanged, the RoCoF metric stays several orders of magnitude below its limit, and the nadir constraint is numerically binding with residuals on the order of 10^{-12} Hz. This indicates that, for the studied demand and wind profiles, synthetic inertia primarily acts as an additional security margin rather than a strong economic driver in the deterministic UC setting.

The comparison between the DC and LSF formulations at $k^{\mathrm{em}} = 4$ s and TCF $= 1.0$ confirms that the PTDF-based LSF model closely reproduces the DC dispatch, cost, and frequency indicators, while achieving smaller optimality gaps. This supports the use of LSFs as a computationally attractive alternative to DC power flow when congestion needs to be represented explicitly. A subsequent TCF analysis with the LSF formulation shows that tightening the transmission-capacity factor from 1.0 to 0.8 has negligible impact on cost, RES spillage, and frequency metrics, whereas a stronger de-rating to TCF $= 0.6$ produces a noticeable cost increase and a small amount of RES curtailment. In all cases, RoCoF and nadir remain numerically secure and no ex-post line overloads are observed, indicating that the additional cost is driven by preventive redispatch to satisfy tighter network limits rather than by frequency violations.

Overall, the results demonstrate that synthetic inertia from wind can be co-optimised with synchronous inertia and LSF-based transmission constraints in a single tractable FCUC model, yielding frequency-secure schedules even under aggressive transmission de-rating. For the La Palma system, the economic effect of synthetic inertia is modest in deterministic UC, but its inclusion provides a structured way to quantify the interplay between inertia provision, wind utilisation, and congestion management.

Future work will extend this framework to stochastic security-constrained UC formulations with scenario-based uncertainty in wind, investigate the viability of this approach on larger test systems, such as the IEEE 96-bus network, and benchmark the analytical nadir approximation against data-driven FCUC formulations. An additional avenue is to couple the proposed FCUC with market-based pricing of inertia and frequency reserves, enabling explicit valuation of synchronous and synthetic inertia in low-inertia island grids.

REFERENCES

[1] Azeez O. Olasoji, D.T.O. Oyedokun, Samuel O. Omogoye, and Chris Thron. Review of frequency response strategies in renewable-dominated power system grids: Market adaptations and unit commitment formulation. *Scientific African*, 26:1–21, 2024.

[2] Azeez O Olasoji, DTO Oyedokun, Mohammad Rajabdorri, and Juan E Sierra-Aguillar. Investigating inclusion of linear sensitivity factors in analytical frequency constrained unit commitment formulation. In *2025 33rd Southern African Universities Power Engineering Conference (SAUPEC)*, pages 1–6. IEEE, 2025.

[3] Mohammad Rajabdorri, Lukas Sigrist, Enrique Lobato, Maria del Carmen Prats, and Francisco M Echavarren. Viability of providing spinning reserves by res in spanish island power systems. *IET Renewable Power Generation*, 15(13):2878–2890, 2021.

[4] Carlos J Ferrandon-Cervantes, Behzad Kazemtabrizi, and Matthias CM Troffaes. Inclusion of frequency stability constraints in unit commitment using separable programming. *Electric Power Systems Research*, 203:107669, 2022.

[5] Mohammad Rajabdorri, Behzad Kazemtabrizi, Matthias Troffaes, Lukas Sigrist, and Enrique Lobato. Inclusion of frequency nadir constraint in the unit commitment problem of small power systems using machine learning. *Sustainable Energy, Grids and Networks*, 36:101161, 2023.

[6] Hamed Ahmadi and Hassan Ghasemi. Security-constrained unit commitment with linearized system frequency limit constraints. *IEEE Transactions on Power Systems*, 29(4):1536–1545, 2014.

[7] Ziyang Zhang, Ershun Du, Fei Teng, Ning Zhang, and Chongqing Kang. Modeling frequency dynamics in unit commitment with a high share of renewable energy. *IEEE Transactions on Power Systems*, 35(6):4383–4395, 2020.

[8] Mingjian Tuo and Xingpeng Li. Security-constrained unit commitment considering locational frequency stability in low-inertia power grids. *IEEE Transactions on Power Systems*, 38(5):4134–4147, 2022.

[9] Cristian Camilo Marín-Cano, Juan Esteban Sierra-Aguilar, Jesús M López-Lezama, Álvaro Jaramillo-Duque, and Juan G Villegas. A novel strategy to reduce computational burden of the stochastic security constrained unit commitment problem. *Energies*, 13(15):3777, 2020.

[10] Cristian Camilo Marín-Cano, Juan Esteban Sierra-Aguilar, Jesús M López-Lezama, Álvaro Jaramillo-Duque, and Walter M Villa-Acevedo. Implementation of user cuts and linear sensitivity factors to improve the computational performance of the security-constrained unit commitment problem. *Energies*, 12(7):1399, 2019.

[11] Mkhutazi Mditshwa, Azeez Olasoji, Komla Folly, and David Oyedokun. Integration of wind power plants for power system frequency stability improvement. In *State-of-the-Art of Mathematical Modeling, Dynamics, and Control of Wind Turbines Engineering*. IntechOpen, 2024.

Authorized licensed use limited to: UNIVERSIDAD PONTIFICIA DE COMILLAS. Downloaded on June 29,2026 at 06:40:54 UTC from IEEE Xplore. Restrictions apply.